INFLUENCE OF GROUND MOTION ON THE TIME EVOLUTION OF BEAMS IN LINEAR COLLIDERS

Andrey SERY *and Olivier NAPOLY
CEA, DSM/DAPNIA
CE-Saclay, F-91191 Gif-sur-Yvette Cedex, France

August 7, 1995

Abstract

This paper resumes a series of investigations devoted to the influence of ground motion on linear colliders in the TeV energy range. We attempt to modelize the variety of measured data about ground motion and then to calculate the behavior of beams in the linear collider affected by this motion. An adequate description of ground motion is found in the form of a two dimensional power spectrum $P(\omega, k)$, that carries information both about time and space dependence of displacements. We then discuss the use of this spectrum to calculate the time evolution of beam position and beam size at the interaction point. An approximation of this spectrum for typical seismic conditions is proposed for a wide range of ω and k based on the results of absolute and relative seismic measurements. Examples of calculations of the time evolution of the beam size and position in the final focus system of a linear collider are presented.

*permanent address: Branch of the Institute of Nuclear Physics, 142284 Protvino, Moscow reg., Russia

Contents

1 Introduction

1.1 Linear colliders

In order to allow effective search of new particles e^+e^- linear colliders envisioned for the future [1] should provide a center of mass energy in the range of 300 GeV - 1 TeV with a luminosity as high as $10^{33} - 10^{34}\,\mathrm{cm}^{-2}\mathrm{s}^{-1}$. Given the expression of the luminosity

$$\mathcal{L} = f_{rep} N^2 / (4\pi \sigma_x^* \sigma_y^*) \tag{1}$$

where f_{rep} is the repetition rate of collisions of the e^+ and e^- bunches, N is the number of particles per bunch and, σ_x^* and σ_y^* are the transverse rms sizes of the bunch at the collision point, the possible set of parameters of the existing projects [2] is as follows: repetition rate $f_{rep} = 10 - 1000$ Hz, number of particles $N = 10^{10} - 10^{11}$, horizontal size $\sigma_x^* = 0.25 - 2$ μm, vertical size $\sigma_y^* = 3 - 30$ nm.

One of the most critical parameters is the extremely small vertical size of the beam at the interaction point and, therefore, the very small required value of the vertical emittance of the beam. A proper alignment of the focusing and accelerating elements of a linear collider is necessary to achieve the high luminosity. The most obvious effect of misaligned focusing lenses is that the e^+ and e^- bunches can simply miss each other at the collision point. Even if the bunches collide, their emittance can be already degraded during acceleration in the linacs or dispersion can appear in the focusing section before collision due to misalignment. This degradation affects in turn the vertical spot size and the luminosity.

The precision of the alignment has to be so high (less than the micrometer) that no conventional technique for position measurement can be used because there is no way to get a reference line with the required precision. The only way seen up to now is to have rough pre-alignment and then to use the bunches themselves as sensors to detect the position of misaligned elements relatively to the desired trajectory of the bunch. Therefore the alignment should be "beam based" and also it should be dynamical (i.e., the alignment should work continuously), because once aligned the collider does not stay aligned forever due to ground motion. A prototype of such a scheme has already been applied on the SLC [3].

The goal of this work is to derive a mathematically consistent model describing ground motion, and to use it to predict the evolution of the beam properties with time over wide range of time intervals – from a few pulses to years– eventually taking the beam based dynamical alignment system into account.

1.2 Ground motion description

When the importance of ground motion for a linear collider was recognized, attempts have been made to get the necessary information to describe this motion. A pioneer work was done at SLAC more than ten years ago [4] to understand

the influence on the 50 GeV SLC linear collider, for which the ground motion was not negligible already. For TeV linear colliders new studies have been made in different places. In Protvino (Russia) investigations of different ground motion characteristics were made six years ago [5] and since then similar studies have been made and are being continued in many other sites (at Novosibirsk [6], CERN [7], KEK [8], DESY [9], Finland [10], SLAC [11] etc.). One can mention also seismic studies performed for large circular colliders like HERA [12] or SSC [13], because some results obtained there can be interesting for a linear collider as well.

Let us briefly describe what kind of measurements have been performed and what kind of information has been obtained in these studies.

All measurements of ground motion can be split in two categories. The first one is the so-called absolute measurements. In this case usually an accelerometer with a pendulum inside is used. It allows to measure acceleration of a single point of the ground surface versus time. If the spectral analysis is then applied, the spectrum of displacements can be obtained from the acceleration spectrum. This method is called absolute measurements because the measurements are made relatively to an object (center of the earth) placed almost infinitely far. The second category consists of the relative measurements. In this case the relative position of two separated points of the surface is measured. Some reference line (strained wire, laser beam, water level in gravity field etc.) must be used in this case. The first method is sometime refined: simultaneous measurements with two distanced and synchronized sensors can give additional information (correlation measurements).

1.2.1 Absolute measurements

Let us consider data treatment methods used in measurements of an absolute motion. Once a time-dependent signal $x(t)$ is measured, one can introduce its dispersion σ as follows:

$$\sigma^2 = \langle x^2 \rangle = \lim_{T\to\infty} \frac{1}{T} \int_{-T/2}^{T/2} x^2(t)dt \tag{2}$$

Here and below we assume that the mean value of the signal is zero $\langle x \rangle = 0$ namely

$$\langle x \rangle = \lim_{T\to\infty} \frac{1}{T} \int_{-T/2}^{T/2} x(t)dt = 0 \tag{3}$$

Performing the spectral analysis of the signal is useful because different vibration frequencies cause different effects on the linear collider. One should note, however, that seismic noise is a random process, so the usual Fourier spectrum

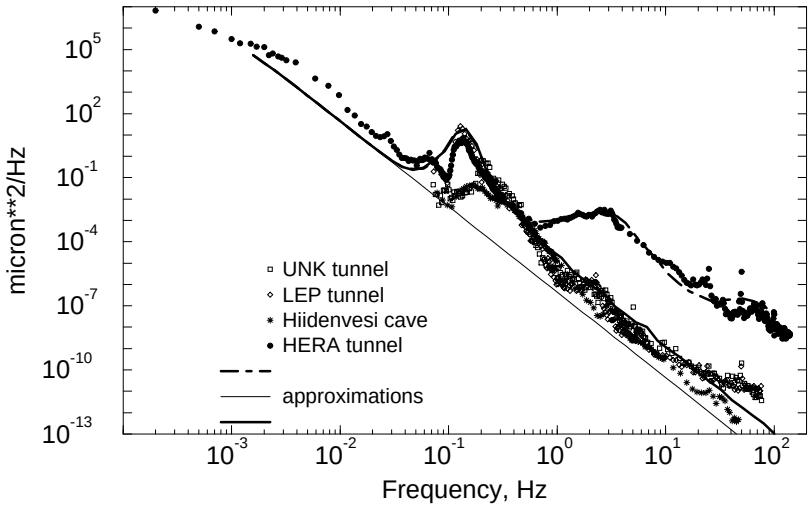

Figure 1: Power spectrum of absolute ground motion. Measured in Protvino (1992), CERN (1993), DESY (1994) and in Finland (1994).

does not exist (it equals to infinity) and the power spectral density (power spectrum in brief) should be considered.

The power spectral density is defined as

$$p(f) = \lim_{T\to\infty} \frac{1}{T} \left| \int_{-T/2}^{T/2} x(t) e^{-i\omega t} dt \right|^2 \tag{4}$$

Here f is frequency, $f = \omega/2\pi$. One of the main properties of the power spectrum is that its integral gives squared dispersion:

$$\sigma^2 = \int_{-\infty}^{\infty} p(f) df \tag{5}$$

In practice the measurement time T is limited and the power spectrum can only be estimated by averaging Fourier spectra obtained from several measurements. The number of averagings fixes the precision on this spectra: it is usually not better than a few percents. Also, the measurement technique with discrete sampling requires to replace the integral by a discrete sum in the formulae. Data measured over time T at sampling frequency f_0 allow to find a spectrum in the range from $1/T$ to $f_0/2$. The dimension of the power density is m^2/Hz if $x(t)$ is the position; sometimes it is more convenient to use $\mu\mathrm{m}^2/\mathrm{Hz}$. This kind of spectra is usually plotted in logarithmic scale because of big changes over the frequency range.

Typical power spectra measured in underground tunnels during quiet time are shown on Fig.1 for different places. On this picture the measurements at Protvino

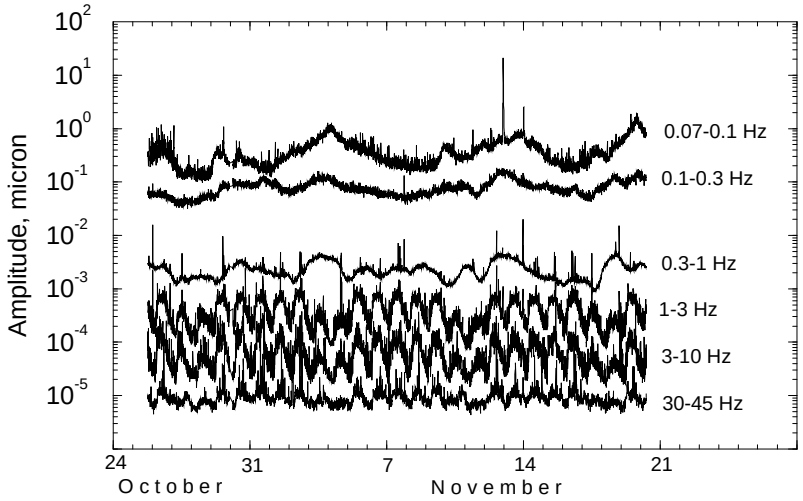

Figure 2: The rms amplitude in different frequency bands versus time. Measured in Finland, October – November 1994.

(Russia) in the 30 m underground tunnel of the UNK storage ring being under construction [5], in the CERN 80 m underground LEP tunnel [7], in the cave situated 40 km from Helsinki in Finland [10] and in the HERA tunnel at DESY [9] are shown. The lines shown on the plot are approximations to be explained later. The frequency band of the data presented on this picture is limited by the working frequency diapason of the sensor, that is the diapason where the ratio of signal to noise of electronics is sufficient. In order to cover a wider frequency band, different sensors with different self-frequencies of pendulum must be used.

The power spectra in Fig.1 grow very fast with decreasing frequency. In quiet conditions they behave approximately as $p(f) \propto 1/f^4$ (compare with the straight line on this picture that corresponds to $1/f^4$). Sources that contribute to the spectrum are different at different frequencies. At very low frequency $f < 1$ Hz the main sources of ground motion are atmospheric activity, water motion in the oceans, temperature variations etc. A famous example of the influence of water motion in the nearest ocean is the peak in the band 0.1-0.2 Hz. This peak, called sometimes as "7-second hum", is generated by the interaction of ocean waves with the coastline: its amplitude depends on the distance from the ocean and on the weather conditions there. In general, vibrations in this low frequency band $f < 1$ Hz depend not only on the local conditions: rather remote sources can give significant contribution to this slow motion.

From the other side, in the band $f > 1$ Hz the human produced noises are usually dominating and the power spectrum depends very much on the local conditions. For example, all except one spectra shown on the Fig.1 were measured during a quiet time (night, minimum of cultural noises). The spectrum measured at DESY presents much bigger amplitudes at $f > 1$ Hz due to noises generated

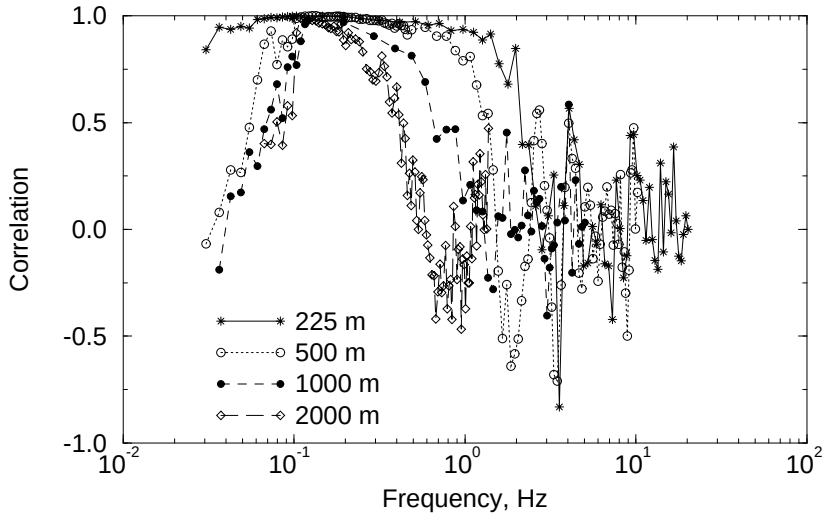

Figure 3: Correlation spectrum of ground motion measured in the CERN LEP tunnel. Distances between sensors are 225, 500, 1000 and 2000 m.

by different technical devices of the HERA collider.

The power spectrum allows to see contributions from different frequencies to the dispersion according to the formula:

$$\sigma^2(f_0 < f < f_1) = \int_{f_0}^{f_1} p(f)df \tag{6}$$

This is illustrated by Fig.2, where the contributions of different frequency bands to the dispersion are shown. This plot is the result of continuous measurements in Finland in the Hiidenvesi cave during October 1994 [10]. In the high frequency part the rms amplitude is one order of magnitude larger during the working hours than during the night time and holidays. Smooth variation of amplitudes in the low frequency part is due to weather variations above the ocean mainly, and sharp isolated peaks are earthquakes, usually remote.

One should note that since the power spectrum of a real signal is symmetrical, it is sufficient to consider only positive frequencies with the proper normalization. On all pictures in this article the measured spectra are defined so that the integral for only positive f in (5) equals to the dispersion (2). However, in all formulae except (6), we will use spectra defined from $-\infty$ to $+\infty$ in such a way that for example (5) is valid.

1.2.2 Correlation measurements

The absolute measurements, performed simultaneously by two sensors, allow to find out the mutual power spectrum of two signals x_1 and x_2 :

$$p_{12}(f) = \lim_{T\to\infty} \frac{1}{T} \int_{-T/2}^{T/2} x_1(t) e^{-i\omega t} dt \int_{-T/2}^{T/2} x_2^*(t') e^{i\omega t'} dt' \tag{7}$$

In contrast with $p(\omega)$ this spectrum is complex. For a real signal $x(t)$ one can write $p_{12}^* = p_{21}$ so that the imaginary part is given by:

$$2\,i\,Im(p_{12}) \;=\; p_{12} \;-\; p_{21} \tag{8}$$

One can note that if characteristics of ground motion do not depend on the location then this imaginary part should be equal to zero. This condition assumed to be always satisfied.

The normalized mutual power spectrum can also be used:

$$N_{12}(f) = \frac{p_{12}}{\sqrt{p_1 p_2}} \tag{9}$$

The real part of N_{12} is called "correlation" and its module is called "coherence". In the frame of the mentioned assumption N_{12} should be equal to its real part.

Perfect correlation between the two points corresponds to $N_{12}(f) = 1$, absence of correlations to $N_{12}(f) = 0$, perfect anticorrelation (phase shift π) to $N_{12}(f) = -1$.

In a simple case when there are only transverse waves with velocity of propagation v, no dissipation and the sources of the waves are remote enough, the correlation (9) will be equal to

$$N_{12}(f) = \cos(c\,\omega L/v) \tag{10}$$

where L is the distance between the probes and c is a coefficient of order one which depends on spatial distribution of the sources of the waves.

An example of the correlation measured in the CERN LEP tunnel [7] is shown on Fig.3. Different curves correspond to different distance between sensors. One can see a good correlation in the low frequency part $f > 0.1$ Hz of the spectrum. At high frequencies the correlation between separated probes disappears. These measurements have shown that the correlation at $f > 0.1$ Hz can be approximated by (10) with the parameter $v(f)$ close to the velocity of sound (about 3000 m/s in that case). At smaller frequency, however, the value $v(f)$ was observed ([5], [7] , [9]) to be much smaller (limited precision of the used probes does not allow to measure the value, however).

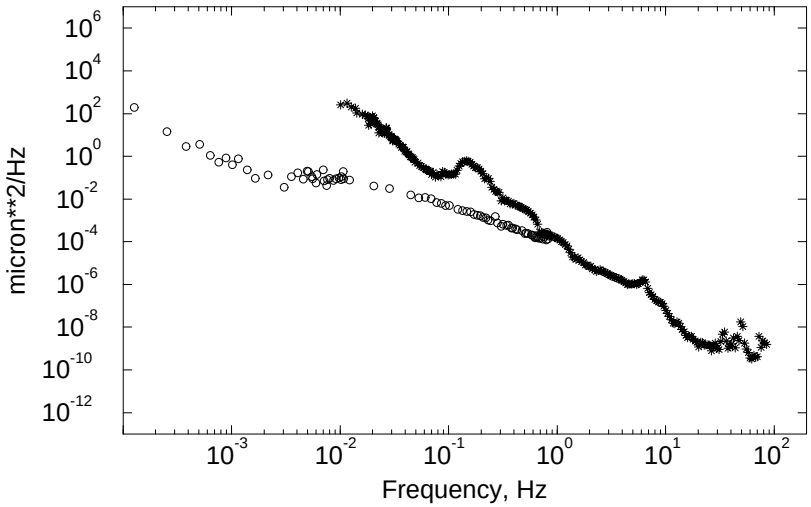

Figure 4: Comparison of the spectrum of relative ground motion (distance 5 m between probes, circles) with the spectrum of absolute ground motion (stars). Measured in the laboratory building in Protvino.

1.2.3 Relative measurements

Measurements of a relative motion give an information about the quantity $x_1(t) - x_2(t)$. The power spectrum $\rho(\omega, L)$ associated to it is given by

$$\rho(\omega, L) = \lim_{T\to\infty} \frac{1}{T} \left| \int_{-T/2}^{T/2} (x_1(t) - x_2(t)) e^{-i\omega t} dt \right|^2 \tag{11}$$

in such a way that

$$\langle [x(t, s+L) - x(t, s)]^2 \rangle = \int_{-\infty}^{\infty} \rho(\omega, L) d\omega/(2\pi) \tag{12}$$

It depends explicitely on the distance L between points of measurements. Note that $\rho(\omega, L)$ and $p(\omega)$ have the same dimension [m^2/Hz].

An example of the spectrum of relative motion of two points separated by 5 m is shown on Fig.4. The measurements were performed in the laboratory building in Protvino using the strained wire technique with pick-up sensors mounted on the tables [14]. On the same plot the results of the absolute measurements at the same place are shown. The amplitudes in this spectrum is large compared with the quiet spectra of Fig.1 because of noisy conditions in the laboratory. One can see that amplitudes of relative motion are much smaller than those of absolute motion at low frequencies. At some high frequency where correlations disappear they starts to be similar.

The previous picture shows results of relative measurements for relatively high frequencies. There is also a lot of data about relative measurements performed with the geodesic technique. The time scale of these data is usually days or years and distances are of the order of hundreds of meters. A typical example of such data is the measurements of the long time scale displacements of the SLC tunnel [19].

It was found in [5] that data about slow relative motion measured in different sites of the world can be described by a simple law:

$$\langle \Delta X^2 \rangle = A \cdot T \cdot L \tag{13}$$

where ΔX is the relative displacement after a time T of the two points separated by a distance L. A is a constant whose value was found to be $A \approx 10^{-4}$ μm^2/sec/m and the variation of this value for different places in the world is not much more than one order of magnitude [5], [15]. This formula (13) is known as the "ATL law".

One can see that the displacement in (13) is proportional to the square root of the time: this stresses the random, diffusional character of the slow relative motion. The square root dependence on the distance L can be understood by supposing that the number of step-like breaks that appears between two points is proportional to the distance between them. There are of course more complex explanations of these dependencies, for example in [16] where a fractal model of ground was developed to explain this behavior.

Although the "ATL law" was found from the direct analysis of measurements of ground motion, its most interesting confirmations come from the observations of beam motion in big accelerators produced by displacements of the focusing elements. For example in [17] the measurements of the motion of the closed orbit in the HERA circular collider have proved this "ATL law" within a wide range of time intervals.

The ranges of T and L where the "ATL law" is valid are very wide. In [15] it was reported that this law is confirmed by measurements in different accelerator tunnels in the range from minutes to tens of years and from a few meters to tens of kilometers.

1.3 Using measured data

Let us discuss now how the available measured data on ground motion can be used for studying the stability of linear collider.

Let us consider the power spectrum of absolute motion. Measurements show (see above) that this spectrum behaves approximately as $p(f) \propto 1/f^4$ in rather wide frequency diapason. One can notice that this spectrum, if it behaves so at low frequencies too, gives an infinite value for the dispersion that is typical of a random signal. This is also true for the difference of the absolute displacements

with finite time separation τ. The associated dispersion is given by the integral:

$$\langle [x(t+\tau) - x(t)]^2 \rangle_t = \int_{-\infty}^{\infty} p(f)\, 2[1 - \cos(\omega\tau)]\, df \tag{14}$$

which is also infinite [1]. Equation (14) shows that the low frequency motion ($\omega \ll 1/\tau$) contributes to the integral with an attenuation factor $(\omega\tau)^2$, but it is still not enough to make the integral finite.

However, for the stability of linear colliders one is only interested in relative displacements between two elements separated by a distance L, and hence in the spectrum of relative motion $\rho(\omega, L)$.

Let us try to obtain this spectrum $\rho(\omega, L)$ from the spectrum of absolute motion. In principle, it can be done if simultaneous absolute measurements by the probe "1" and probe "2" are performed. These spectra are connected as follows:

$$\rho(\omega, L) = p_1(\omega) + p_2(\omega) - p_{12}(\omega, L) - p_{21}(\omega, L) \tag{16}$$

where p_1 ,p_2 and p_{12} ,p_{21} are the usual and mutual spectra. Assuming that the spectra of these two signals are the same $p_1 = p_2 = p(\omega)$, one can rewrite (16) using definition of the correlation as:

$$\rho(\omega, L) = p(\omega)\, 2\, [1 - Re\, (N_{12}(\omega, L))] \tag{17}$$

At first sight it seems that the spectrum of relative motion can be extracted from the spectrum of absolute motion using (17). But in practice it is only possible at high frequencies where the correlation is close to zero, and $\rho(\omega, L) \approx 2\, p(\omega)$. A problem appears at low frequencies where the correlation is close to one: the correlated part of motion has usually a much bigger amplitude that the uncorrelated part. So, because of the limited accuracy of sensors, the correlation cannot be measured with the necessary precision and the formula (17) cannot be used.

The spectrum of relative motion can be obtained, of course, directly from relative measurements. The problem here is that the measurements can be performed only in some limited region of parameters (frequency or distance). For example, measurements with water level system give information only about slow motion. The strained wire technique can measure fast vibrations also, but the distance

[1] This formula can be obtained using the parity of $p(f)$ and the fact that the autocorrelation $\langle x(t+\tau)\, x(t) \rangle_t$ and the power spectrum are connected via Fourier transformation:

$$\lim_{T\to\infty} \frac{1}{T} \int_{-T/2}^{T/2} x^*(t) x(t+\tau) dt = \int_{-\infty}^{\infty} p(f) e^{i\omega\tau} df \tag{15}$$

between measured points is limited for this method as for the previous one too. Optical methods have problems of accuracy over long distances etc. So there is no ideal instrument for measuring the characteristics of ground motion. Therefore both absolute and relative measurements should be used in complement to each other in order to cover a wider range of parameters.

There is one essential drawback with using the spectrum of relative motion: it does not separate contributions from different spatial wavelengths to the relative motion of two points. These contributions may have very different impact on the linear collider stability especially for wavelengths close to harmonics of betatron wavelengths.

This is the main reason why a new mathematical tool describing ground motion has to be built which incorporates both results from absolute and relative measurements and at the same time is adequate to calculate beam stability in linear colliders.

2 Generalized description of ground motion

2.1 Two dimensional power spectrum of ground motion

As already mentioned, TeV linear colliders are very sensitive to ground motion. But, of course, if ground motion would displace the linear collider as a whole rigid body, it would not influence its operation. Rather smooth changes of the shape of the collider are not dangerous too. For example, vibrations with long spatial periods like waves from the ocean have a very small influence on the linear collider in spite of their big amplitudes. From the other side, vibrations with spatial periods of a few tens of meters can be dangerous, even though their amplitudes are much smaller. Thus, it is necessary to have informations about both time and spatial characteristics of ground motion. An adequate description of ground motion is through the two dimensional power spectrum proposed in [10].

Let us denote s the longitudinal position of an element along linear collider and $x(t,s)$ the transverse position of this element, which depends also on the time t. The displacement $x(t,s)$ is an absolute one, i.e. it is measured relatively to an infinitely remote object. We consider only transverse displacements of elements because they are known to have the most significant influence on linear collider.

One can introduce a two dimensional power spectrum of this displacement $x(t,s)$ as:

$$P(\omega,k) = \lim_{T\to\infty}\lim_{L\to\infty}\frac{1}{T}\frac{1}{L}\left|\int_{-T/2}^{T/2}\int_{-L/2}^{L/2} x(t,s)\,e^{-i\omega t}e^{-iks}dt\,ds\right|^2 \qquad (18)$$

where $k = 2\pi/\lambda$ and λ is the spatial period of displacements. We will see later that this spectrum contains all the necessary information for a linear collider.

The two dimensional spectrum (18) contains informations both about relative and absolute motions. For example, it is related to the one dimensional spectrum by the formula

$$p(\omega) = \int_{-\infty}^{\infty} P(\omega, k)\ dk/(2\pi) \tag{19}$$

The value of dispersion of the displacement $x(t, s)$ is then given by

$$\sigma^2 = \int_{-\infty}^{\infty} \int_{-\infty}^{\infty} P(\omega, k)\, d\omega\, dk/(2\pi)^2 \tag{20}$$

It should of course be infinite as it is for the usual spectrum too, since the integral extends down to $\omega = 0$.

Other spectral characteristics can be determined from this two dimensional power spectrum. For example, the real part of the normalized mutual power spectrum (9) for two points separated by the distance L is equal to

$$Re(N_{12}(\omega)) = \frac{\int_0^{\infty} P(\omega, k)\ \cos(kL)\, dk}{\int_0^{\infty} P(\omega, k)\, dk} \tag{21}$$

For a linear collider we have to know the behavior of relative displacements of two elements of the collider. Let us assume for simplicity that at the beginning ($t = 0$) the collider is perfectly aligned and let us introduce the misalignment after the time T: $X(T, s) = x(t = T, s) - x(t = 0, s)$. Then the dispersion of the relative misalignment over a distance L and after a time T is given by

$$\sigma^2(T, L) = \langle [X(T, s + L) - \ X(T, s)]^2 \rangle = \int_{-\infty}^{\infty} \int_{-\infty}^{\infty} P(\omega, k)\, 2[1 - \cos(\omega T)]\, 2[1 - \cos(kL)]\, d\omega\, dk/(2\pi)^2 \tag{22}$$

This is a main formula to evaluate linear collider stability with the help of the two dimensional power spectrum.

2.2 Approximation of the two dimensional power spectrum based on measured data of ground motion

Unlike the absolute $p(\omega)$ and relative $\rho(\omega, L)$ power spectra the two dimensional power spectrum $P(\omega, k)$ is not directly measured in an experiment. But if one

knows $p(\omega)$ and $\rho(\omega, L)$ for a wide enough range of parameters, one can determine the two dimensional power spectrum through the following identities:

$$\rho(\omega, L) = \int_{-\infty}^{\infty} P(\omega, k)\, 2[1 - \cos(kL)]\, dk/(2\pi) \tag{23}$$

and, for the back transformation:

$$P(\omega, k) = \int_{0}^{\infty} \cos(kL)\ [\rho(\omega, L = \infty) - \rho(\omega, L)]\ dL \tag{24}$$

In (24) $\rho(\omega, L = \infty)$ is equal to $2\,p(\omega)$ (see (17)) because correlations vanish at $L = \infty$.

Let us consider the two dimensional spectrum that corresponds to the motion described by the "ATL law" (13). It can be written as

$$P(\omega, k) = \frac{A}{\omega^2 k^2} \tag{25}$$

which can be easily shown by direct substitution of (25) into (22) and comparison with (13). The relative spectrum $\rho(\omega, L)$ for the "ATL law" is then given by:

$$\rho(\omega, L) = \frac{A \cdot L}{\omega^2} \tag{26}$$

We are going to use this formula as an approximation of $\rho(\omega, L)$ in the region of parameters where it does not contradict measured data or where it is known to work. This formula can be used as an approximation of $\rho(\omega, L)$ only in the region of small frequencies, because it behaves like $1/\omega^2$ while the spectrum of absolute motion in a quiet place behaves like $1/\omega^4$. Thus for some high frequencies (26) will contradict to the condition $\rho(\omega, L) \leq 2\,p(\omega)$ which follows from (17).

From the other side, we know from correlation measurements that for some distance L there are no correlations for some band in the high frequency region. Thus one can use the absolute spectrum as an approximation to $\rho(\omega, L)$ in this region of parameters: $\rho(\omega, L) = 2\,p(\omega)$. One can take $p(\omega) = B/(2\omega^4)$ as an approximation for a quiet place (see Fig.1).

Let us take these two approximations with the border between them corresponding to $B/\omega_0^4 = A \cdot L/\omega_0^2$:

$$\begin{aligned} \rho(\omega, L) &= \frac{A \cdot L}{\omega^2} \quad , \quad 0 < \omega < \omega_0 \\ \rho(\omega, L) &= \frac{B}{\omega^4} \quad , \quad \omega_0 < \omega < \infty \end{aligned} \tag{27}$$

where $\omega_0 = (B/(A \cdot L))^{1/2}$. From Eq.(27) one then obtains the following approximation for the power spectrum $P(\omega, k)$:

$$P(\omega, k) = \frac{A}{\omega^2 k^2}(1 - \cos(L_0 k)) \tag{28}$$

with $L_0 = B/(A \cdot \omega^2)$. In the rest of the paper we will use this approximation as a model for "quiet seismic conditions" with $A = 10^{-4}$ μm^2/sec/m for the parameter of the ATL law, and $B = 10^{-3}$ μm^2/sec^3 for the parameter of the spectrum of absolute motion, a typical value for a quiet place.

The exact result for the dispersion of the relative misalignment corresponding to this model is then given, from Eq.(22), by

$$\begin{aligned}\langle \Delta X^2 \rangle \quad &= A \cdot T \cdot L \; + \; A \cdot T \cdot L \, \tfrac{2}{\pi} \left(Si(2x_0) - \tfrac{1-\cos(2x_0)}{2x_0} \right) + \\ &+ \tfrac{BT^3}{6\pi} \left(2Si(2x_0) + \tfrac{\cos(2x_0)}{x_0} + \tfrac{\sin(x_0) * (\sin(x_0) + x_0 \cos(x_0))}{x_0^3} \right) \end{aligned} \tag{29}$$

where $x_0 = T/2 \sqrt{B/(L \cdot A)}$ and $Si(x)$ is defined as

$$Si(x) = -\int_x^\infty \frac{\sin(t)}{t} dt \tag{30}$$

One can show from this formula that the chosen form of the $P(\omega, k)$ spectrum gives a square root dependence of the relative misalignment versus time for large T (corresponding to the "ATL law"):

$$\langle \Delta X^2 \rangle = A \cdot T \cdot L \qquad T \gg T_0 \tag{31}$$

while for small T the relative misalignment is just proportional to the time T:

$$\langle \Delta X^2 \rangle = A \cdot T^2 \cdot L \, / T_0 \qquad T \ll T_0 \tag{32}$$

where $T_0 = \pi/2 \sqrt{A \cdot L/B}$.

In fact, with a reasonable accuracy one can use the following simple formula

$$\langle \Delta X^2 \rangle \approx A \cdot T \cdot L \, \frac{T}{T + T_0} \tag{33}$$

as an approximation of (29).

2.3 Improvements of the approximation

Let us compare the measured correlation with the one calculated from the approximation of $P(\omega, k)$ expressed by (28). Using (21) and (28) one can show that the correlation disappears for $\omega^2 > B/(A \cdot L)$. This contradicts the measured data at least in the region 0.1 Hz$< f <$ 100 Hz, where a linear dependence of the cut frequency on the distance L has been observed [5] , [7]. The reason of this contradiction could be the fact that contributions of elastic waves (like waves from the ocean, for example) are not included in the power spectrum. An elastic wave of a given frequency ω may be added to the spectrum $P(\omega, k)$ with some distribution on the wave number k from 0 to k_{max}; the case $k = 0$ corresponds to

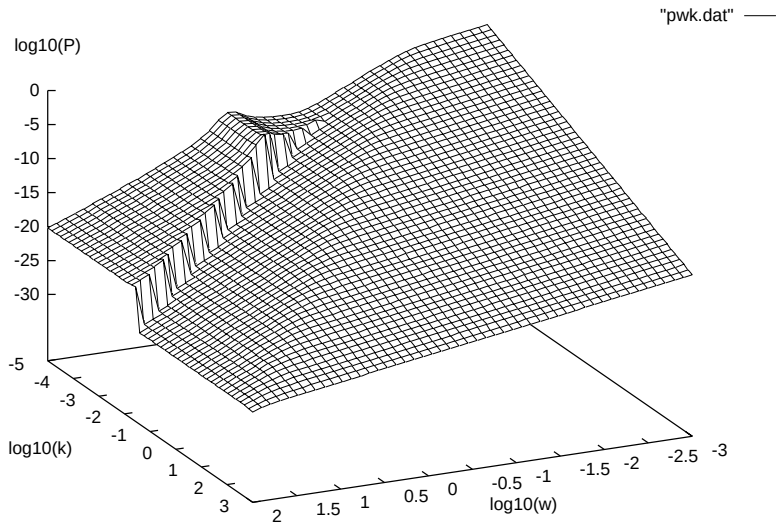

Figure 5: 3-d plot of the approximation of the two dimensional power spectrum with additional contribution of elastic waves.

wave going perpendicular to the linear collider (transverse waves), and $k = k_{max}$ corresponds to the wave traveling along the collider. Let us add the effect of this kind of waves to (28) in the following way:

$$P(\omega, k) = \frac{A}{\omega^2 k^2}(1 - \cos(L_0 k)) \ + \ D(\omega) \cdot U(k, k_{max}) \tag{34}$$

The function $U(k, k_{max})$ describes the wave number distribution of the waves with frequency ω. The following expression:

$$U(k, k_{max}) = \begin{cases} \frac{2}{\sqrt{k_{max}^2 - k^2}} & \text{if } |k| \leq k_{max} \\ 0 & \text{if } |k| > k_{max} \end{cases} \tag{35}$$

corresponds to transverse waves propagating at the surface of the ground with uniform distribution over azimuthal angle, with $k_{max} = \omega / v_o$ and v_o the velocity of wave propagation.

Since the integral over $dk/(2\pi)$ of $U(k, k_{max})$ equals one, the function $D(\omega)$ describes contribution of these waves to the absolute spectrum $p(\omega)$. Writing $D(\omega)$ as

$$D(\omega) = \frac{a_o}{1 + [d_o(\omega - \omega_o)/\omega_o]^4} \tag{36}$$

allows one to take into account the peak of the waves from the oceans and also, because of the $1/\omega^4$ dependence, to add some wave contribution at high frequencies. To reproduce the spectrum corresponding to quiet conditions, like in the LEP or UNK tunnels, we consider the following parameters: $\omega_o = 2\pi * 0.14$ Hz

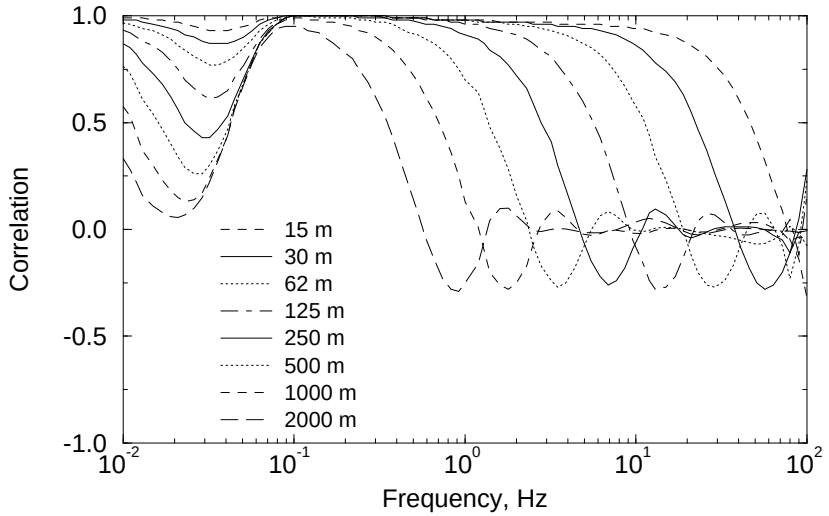

Figure 6: Correlation function $N_{12}(\omega, L)$ for different distances calculated with the analytic model of $P(\omega, k)$ for quiet UNK or LEP tunnel conditions.

for the frequency of the peak, $a_o = 10\mu\text{m}^2/\text{Hz}$ for its amplitude and $d_o = 5$ for its width, and, $v_o = 3000$ m/s for the velocity. The resulting approximation of the two dimensional spectrum $P(\omega, k)$ is shown on Fig.5 (with the $(1 - \cos(\xi))$ term in (34) replaced by $1/(1 + 2/\xi^2)$ to smooth the plot). The absolute power spectrum calculated from this analytic form of $P(\omega, k)$ is plotted in Fig.1 as a solid line: one can see that it is in good agreement with the LEP and UNK power spectra. Also, the correlation function $N_{12}(\omega, L)$ plotted on Fig.6 exhibits a decreasing of the correlation in the region $f = 0.01 - 0.1$ Hz which was observed in measurements ([5], [7], [9]) but not understood completely. In the framework of our model, this behavior of correlations can be explained by the fact that below 0.1 Hz there is no more significant sources of elastic waves.

One can also build an approximation for $P(\omega, k)$ which corresponds to seismic conditions with big contributions from cultural noises (as in the HERA tunnel [9]). In this case we introduce the three additional peaks with the following parameters: $\omega_o = 2\pi * 0.14$ Hz, $a_o = 10\mu\text{m}^2/\text{Hz}$, $d_o = 5$, $v_o = 1000$ m/s for the first peak, $\omega_o = 2\pi * 2.5$ Hz, $a_o = 10^{-3}\mu\text{m}^2/\text{Hz}$, $d_o = 1.5$, $v_o = 400$ m/s for the second, $\omega_o = 2\pi * 50$ Hz, $a_o = 10^{-7}\mu\text{m}^2/\text{Hz}$, $d_o = 1.5$, $v_o = 400$ m/s for the third. The thick dashed line on Fig.1 shows the spectrum of absolute motion, calculated from $P(\omega, k)$, corresponding to these parameters. The parameters a_o and d_o have been chosen to fit the absolute spectrum, while the parameter v_o has been derived [22] from correlation measurements at the HERA tunnel [23] and measurements of the closed orbit motion in HERA [17].

One can conclude that some additional data allows to build an approximation of the $P(\omega, k)$ based on (28) corresponding to local conditions with a reasonable accuracy. At some point improving this accuracy would be useless because of

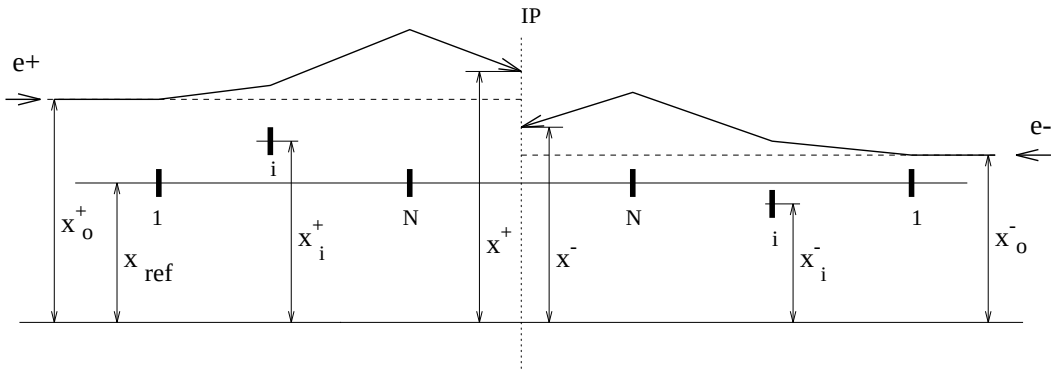

Figure 7: Layout of the e^+ and e^- parts of a linear collider near interaction region.

the uncertainty about conditions in which the linear collider will be operating. Variations of local conditions seem to be larger than the uncertainty of the approximations. For example the constant A can vary by about one order of magnitude in different places and the level of cultural noise may be very different as well. Nevertheless we believe that the two approximations for the power spectrum of very quiet and very noisy places should be useful to investigate the beam stability in a given collider design.

3 Calculation of beam behavior using the two dimensional power spectrum

In this section we want to show how the two dimensional power spectrum $P(\omega, k)$ can be used to describe the beam stability in a linear collider. We will restrict ourselves to the effects of displacements at the leading linear order on the relative beam offset and at the leading quadratic order on the beam spot size at the IP.

3.1 Beam offset at the IP

We consider two sections of the linear collider which are symmetrical relative to the IP (see Fig.7). We assume that both channels have been perfectly aligned at the time $t = 0$ on some reference coordinate[2] $x_{\rm ref}$. Let x_i^+ be the transverse position of the focusing element i on the e^+ side and x_i^- on the e^- side measured at some later time T relative to some reference line as shown on Fig.7. The elements are enumerated from the entrance of each channel, the first element having number 1 and the last before the IP number N. We assume that the positions of the beams at injection x_0^+ and x_0^- are related to the position of some

[2]This reference coordinate $x_{\rm ref}$ may vary along the line: this does not affects the main results of this paragraph.

element, say a beam position monitor, at the entrance of the considered section[3]. With this assumption, the time evolution of all the coordinates $(x_i^{\pm})_{i=0,N}$ can be described by the 2d-power spectrum like in Eq.(22)

$$\langle [x_i^{\pm}(T) - \quad x_j^{\pm}(T)]^2 \rangle = \int_{-\infty}^{\infty} \int_{-\infty}^{\infty} P(\omega,k)\, 2[1-\cos(\omega T)] \\ 2[1-\cos(k(s_i^{\pm}-s_j^{\pm})]\, d\omega\, dk/(2\pi)^2 \tag{37}$$

where $s_i^{\pm}$ is the longitudinal position of the i-th element in the e^+ and e^- beam lines.

The most harmful effect of focusing element displacements for the luminosity is the transverse offset $(x^+ - x^-)$ of the opposite beams at the IP. Let a_i be the first derivative of the beam transverse displacement at the IP with respect to the displacement of the element i. At the first order, the e^+ and e^- beam offsets at the IP are given by

$$(x^{\pm} - x_{\rm ref}) = R_{11}(x_0^{\pm} - x_{\rm ref}) + \sum_{i=1}^{N} a_i (x_i^{\pm} - x_{\rm ref}) \tag{38}$$

where R is the transfer matrix of the section. We have assumed that the coefficients a_i are the same for the e^- and for the e^+ parts. They can be easily calculated using optical functions of the channel. For example for a short quadrupole, $a_i = k_i r_{12}$ where k_i is the integrated strength of the quadrupole and r_{12} is the element of transfer matrix from this element to the IP (for horizontal displacements, for the vertical one should take r_{34}). By considering a rigid displacement of the whole beam line, with $x_0 = x_i = x$, it is easy to show that they satisfy the identity

$$\sum_{i=1}^{N} a_i = 1 - R_{11} \tag{39}$$

Since only the relative displacement of the beams at the IP influences the luminosity, one can write for this relative offset:

$$x^+ - x^- = \sum_{i=0}^{N} a_i (x_i^+ - x_i^-) \tag{40}$$

with the notation

$$a_0 = R_{11} \tag{41}$$

The mean value $\langle x^+ - x^- \rangle$ is equal to zero. The mean square value is given by:

$$\langle (x^+ - x^-)^2 \rangle = \sum_{i=0}^{N} \sum_{j=0}^{N} a_i a_j \langle (x_i^+ - x_i^-)(x_j^+ - x_j^-) \rangle \tag{42}$$

[3]The case where the beam is injected with an angle is not considered in this paper.

To relate the above expression to square dispersions calculated from the 2d-spectrum by Eq.(37), one uses the following identity

$$(x_1 - x_2)(x_3 - x_4) = \frac{1}{2}\left[(x_1 - x_4)^2 + (x_2 - x_3)^2 - (x_1 - x_3)^2 - (x_2 - x_4)^2\right] \quad (43)$$

Assuming that the spectrum $P(\omega, k)$ is homogeneous in such a way that $\langle (x_i^+ - x_j^+)^2 \rangle = \langle (x_i^- - x_j^-)^2 \rangle$ and $\langle (x_i^+ - x_j^-)^2 \rangle = \langle (x_i^- - x_j^+)^2 \rangle$, one gets for the rms of the relative beam offset

$$\langle (x^+ - x^-)^2 \rangle = \sum_{i=0}^{N} \sum_{j=0}^{N} a_i a_j \left(\langle (x_i^+ - x_j^-)^2 \rangle - \langle (x_i^+ - x_j^+)^2 \rangle \right) \quad (44)$$

Combining this expression with Eq.(22) allows one to calculate, from a given model of the 2d-power spectrum $P(\omega, k)$, the time evolution of the rms relative offset after the time $t = 0$ when it is zero.

For a pure "ATL" motion it is simply given by:

$$\langle (x^+ - x^-)^2 \rangle = AT \sum_{i=0}^{N} \sum_{j=0}^{N} a_i a_j \left(|s_i^+ - s_j^-| - |s_i^+ - s_j^+| \right) \quad (45)$$

In general, Eq.(44) can be expressed as

$$\langle (x^+ - x^-)^2 \rangle = \int_{-\infty}^{\infty} \int_{-\infty}^{\infty} P(\omega, k)\, 2[1 - \cos(\omega T)]\, G(k)\, \frac{d\omega}{2\pi}\, \frac{dk}{2\pi} \quad (46)$$

with the spectral function $G(k)$ given by

$$G(k) = \sum_{i=0}^{N} \sum_{j=0}^{N} 2\, a_i a_j \left(\cos(k(s_i^+ - s_j^+)) - \cos(k(s_i^+ - s_j^-)) \right) \quad (47)$$

By taking the origin of the longitudinal coordinate $s = 0$ at the IP, one has $s_i^+ = -s_i^-$ and the above expression simplifies to

$$G(k) = 4 \left(\sum_{i=0}^{N} a_i \sin(k s_i^+) \right)^2 \quad (48)$$

The positive function $G(k)$ describes the spectral response to harmonic excitations of spatial period of $2\pi/k$, of the considered focusing section in terms of relative displacement of beams at the IP. For large k it fluctuates around N (if all $|a_i| \approx 1$). For harmonics with long wavelengths it is proportional to k^2, except when $R_{12} = 0$ which is the most interesting case of beam lines with a phase advance equal to a multiple of π. Indeed one can easily show by tilting the

whole beam line by a constant angle x'_0 that the coefficients a_i verify to a good approximation - namely for thin lenses - the following identity

$$\sum_{i=0}^{N} a_i s_i + R_{12} = s_{\rm IP} \tag{49}$$

Since we took $s_{\rm IP} = 0$ in Eq.(48), one gets for small k

$$G(k) \simeq 4\left(kR_{12} + {\rm O}(k^3)\right)^2 \tag{50}$$

showing that the spectral function $G(k)$ behaves as k^6 for $k \to 0$ if $R_{12} = 0$.

Once $G(k)$ has been calculated for a given focusing structure Eq.(46) is useful for comparing the behavior of beams through this structure in different seismic conditions. It also allows one to calculate the effect of different parts of the spatial wave-number spectrum.

3.2 Beam spot size at the IP

Transverse displacements of focusing elements can generate other effects at the IP. For example, for the final focus system of a linear collider the next most important effect is the spot size growth at the IP induced by dispersion, longitudinal shift of the beam waists and xy-coupling generated by offset beams in quadrupoles and sextupoles. At the first order in the normalized transfer matrix error at the IP

$$\delta Q = \delta R \cdot R^{-1} \tag{51}$$

the vertical spot size growth is given by[4]

$$\frac{\delta\sigma_y^*}{\sigma_y^*} = \frac{1}{2}\left[\left(\frac{\delta Q_{34}}{\beta_y^*}\right)^2 + \left(\frac{\delta Q_{31}\,\sigma_x^*}{\sigma_y^*}\right)^2 + \left(\frac{\delta Q_{32}\,\sigma_x^*}{\sigma_y^*\beta_x^*}\right)^2 + \left(\frac{\delta Q_{36}\,\sigma_\delta}{\sigma_y^*}\right)^2\right] \tag{52}$$

The first term corresponds to the β_y waist-shift generated by quadrupole and sextupole horizontal displacements. The second and third terms correspond to xy and $x'y$ couplings, and the fourth term to vertical dispersion generated by quadrupole and sextupole vertical displacements.

The spot size growth induced by these effects can be calculated as for the offset in Eq.(44) but with different coefficients. For instance, the vertical dispersion δQ_{36} can be written as follows

$$\eta_y^* = \delta Q_{36} = T_{336}(y_0 - y_{\rm ref}) + \sum_{i=1}^{N} b_i\,(y_i - y_{\rm ref}) \tag{53}$$

[4]The linear contribution from the vertical demagnification error δQ_{33} is usually negligible.

Again a constant translation of the whole beam line leads to the identity

$$\sum_{i=1}^{N} b_i = -T_{336} \tag{54}$$

in such a way that the dispersion error is given by

$$\delta Q_{36} = \sum_{i=1}^{N} b_i \left(y_i - y_0\right) \tag{55}$$

As for the offset rms, the dispersion rms error is then related to the 2d-power spectrum through the following equality

$$\langle (\delta Q_{36})^2 \rangle = \frac{1}{2} \sum_{i=1}^{N} b_i b_j \left(\langle (y_i - y_0)^2 \rangle + \langle (y_j - y_0)^2 \rangle - \langle (y_i - y_j)^2 \rangle \right) \tag{56}$$

This expression can also be used to defined a spectral function $G_\eta(k)$ associated to the dispersion:

$$G_\eta(k) = \sum_{i=1}^{N} \sum_{j=1}^{N} b_i b_j \left(1 - 2\cos(k(s_i - s_0)) + \cos(k(s_i - s_j))\right) \tag{57}$$

By applying the same treatment to the other error terms in Eq.(52) and by summing them with the dispersion term, the time evolution of the vertical spot size of one beam can be calculated from the 2d-power spectrum $P(\omega, k)$. Since the horizontal displacements are responsible for the degradation of the spot size induced by the waist-shift δQ_{34} term, we will assume in the next section that the horizontal and vertical ground motions are described by the same power spectrum.

4 Application to final focus systems

The final focus system (FFS) of a linear collider is the special optical system placed immediately before IP. It provides the required big demagnifications of the transverse beam dimensions down to the desired beam sizes at collision. Its optics is based on the SLC final focus system [20, 21]. Big demagnifications result in strong focusing of the beam which in turn leads to large chromatic aberrations. These aberrations are compensated in chromatic correction sections using bending magnets and sextupoles. Usually a final focus system has a first telescope, two dispersive FODO sections for correction of the horizontal and vertical chromaticities, and a final telescope. The tightest tolerances to transverse magnet displacements are found in the FFS (last quads, sextupoles). It is therefore natural to illustrate the use of the above formalism to describe the influence of ground motion on such systems.

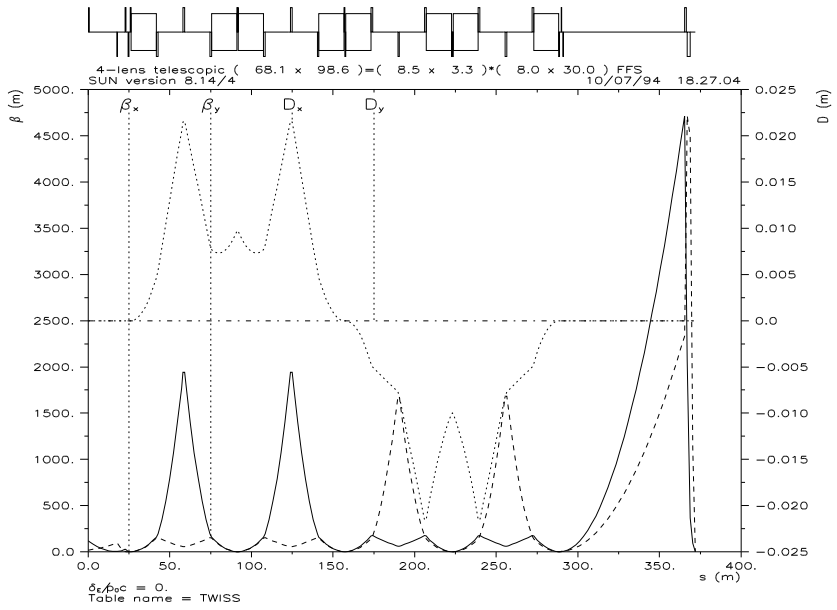

Figure 8: Layout and optics functions of the TESLA FFS

An example of a FFS optics with magnet layout and betatron functions for TESLA [18] is shown in Fig.8. The relevant beam parameters at the IP of some existing linear collider projects are shown in Table 1 for a final beam energy of 250 TeV [2]. $\beta^*_{x,y}$ are the beta functions and $\sigma^*_{x,y}$ the rms transverse beam size at the IP, σ_z is the rms bunch length, σ_δ the rms relative energy spread within one bunch or one bunch train, and f_{rep} the repetition frequency of the bunch trains. Usually the repetition rate of collisions within the same train in the multibunch case is too high for the trajectory of a single bunch to be corrected separately. For TESLA, however, this repetition rate (shown in brackets) may be small enough to allow some fast bunch to bunch correction scheme. One can see from Table 1 that the vertical beam sizes at the IP are much smaller than the horizontal ones. We therefore concentrate on the time stability of the vertical offset and spot size which are expected to set the most severe tolerances on displacements.

	TESLA	SBLC	VLEPP	CLIC
$\beta^*_{x,y}$ [mm]	25 , .7	22 , .8	100,.2	10 , .18
$\sigma^*_{x,y}$ [nm]	845 , 19	678 , 30	2000 , 6	250 , 7.5
σ_z [mm]	.7	0.5	0.75	0.2
f_{rep} [Hz]	5 (1.4×10^6)	50	300	3200
$\sigma_\delta[10^{-3}]$	1	5	5	2

Table 1: Beam parameters at the IP for some final focus systems

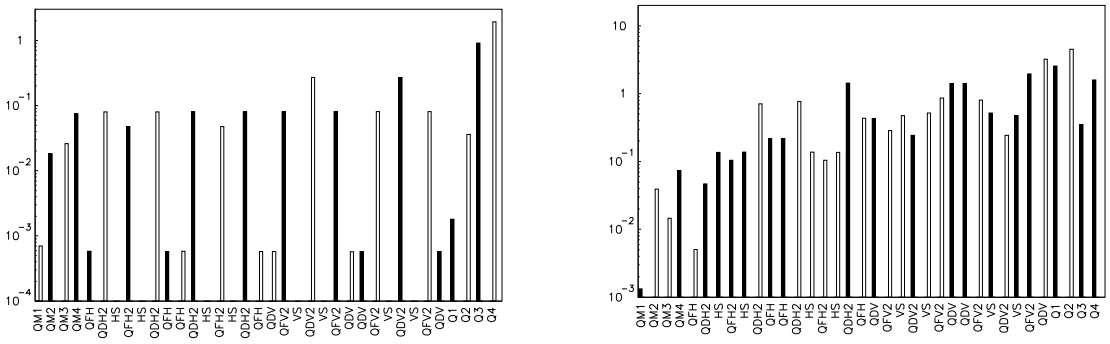

Figure 9: Coefficients a_i (left) and b_i (right) for the vertical displacement and vertical dispersion of the beams at the IP of the TESLA FFS. White bars correspond to positive values, black bars to negative ones.

4.1 Beam stability for typical quiet seismic conditions

The linear response of the FFS optics to ground motion is mainly characterized by the coefficients a_i and b_i defined above, namely the ratio of the vertical beam offset and dispersion at the IP to the vertical displacement of each magnet indexed by i. These coefficients are plotted in Fig.9 for each magnet of the TESLA FFS. One can see from these plots that the main contribution to the beam displacement at the IP comes from the two last quadrupoles, while the main sources of dispersion errors are the first two lenses of the last telescope. Calculated from

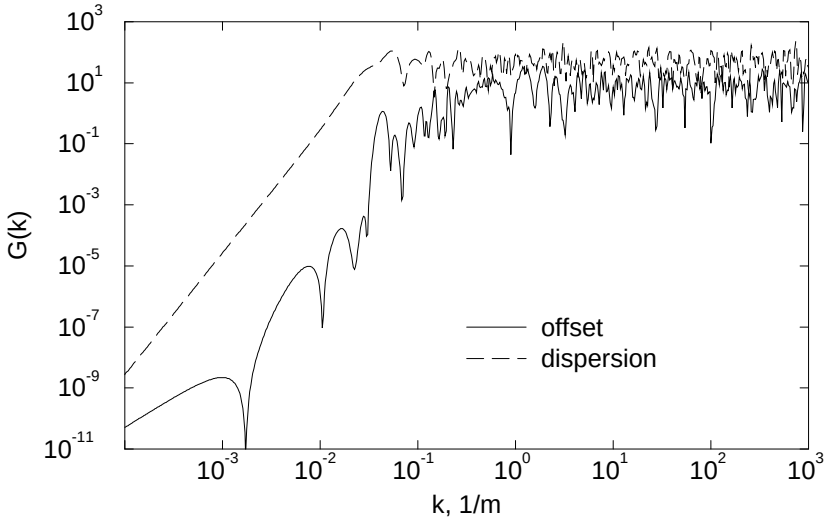

Figure 10: Spatial spectral functions $G(k)$ and $G_\eta(k)$ for the TESLA FFS.

these coefficients with Eqs.(48,57), the spatial spectral functions $G(k)$ and $G_\eta(k)$ associated to the vertical relative offset and dispersion are plotted in Fig.10. For small k, $G_\eta(k)$ behaves as k^4 and $G(k)$ exhibits the k^6 behavior predicted in

	TESLA	SBLC	VLEPP	CLIC
$N_{\delta y}$	1 (1.8×10^5)	15	15	220
$N_{\sigma_y^*}$	210	650	540	16600

Table 2: Number of pulses corresponding to 2% luminosity loss due to vertical offset (N_{δ_y}) or vertical spot size growth ($N_{\sigma_y^*}$) at the IP of different projects.

Eq.(50) over a small range only.

The time evolution of the relative beam offset, the vertical beam dispersion and spot size at the IP are shown on Figs.11, 12 and 13 assuming a perfectly aligned system at $t = 0$. They are calculated as explained in the preceding section from the 2-d power spectrum $P(\omega, k)$ corresponding to the quiet seismic conditions given by Eq.(28). The offset and dispersion curves are very close because of the similarity of the FFS designs. From the relative offset and spot size variations one can derive the time corresponding to a loss of luminosity of 2% induced by either of these effects[5]. Then from the repetition rate given in Table 1, one gets the corresponding number of pulses, reported in Table 2.

One can see from this table that, except for CLIC, the number of pulses corresponding to 2% luminosity loss due to beam offset caused by ground motion is very small. It means that a fast correction is necessary to keep beams head on at the interaction point. For TESLA a fast correction within each train seems to be required: the number of bunches in a train colliding before 2% luminosity is lost, given in brackets, then exceeds largely the total number of bunches in the train. One should say however that the relative offset of the beams is due at 90% to the relative motion of the two opposing final doublets. One may hope that these four quadrupoles, separated by less than ten meters, will be placed on some stabilized support.

If the offset of the beams at the IP is corrected by a fast correction scheme, the luminosity degradation is due the growth of the beam spot size. The number of pulses before 2% luminosity loss is then of the order of one thousand. Another correction scheme is required to realign the elements of the FFS.

4.2 Effect of different seismic conditions

Besides of the power spectrum typical of quiet sites used above, we have introduced in Sect.2.3 a model for the power spectrum of the HERA tunnel with a high level of cultural noise (cf. Fig1). In fact, to account for the recent measurement of the constant A entering the ATL law made at HERA [17], we should also consider a third model obtained by taking $A = 10^{-5}$ μm^2/sec/m, that is

[5]The tolerances to offset do not take the beam-beam attraction into account.

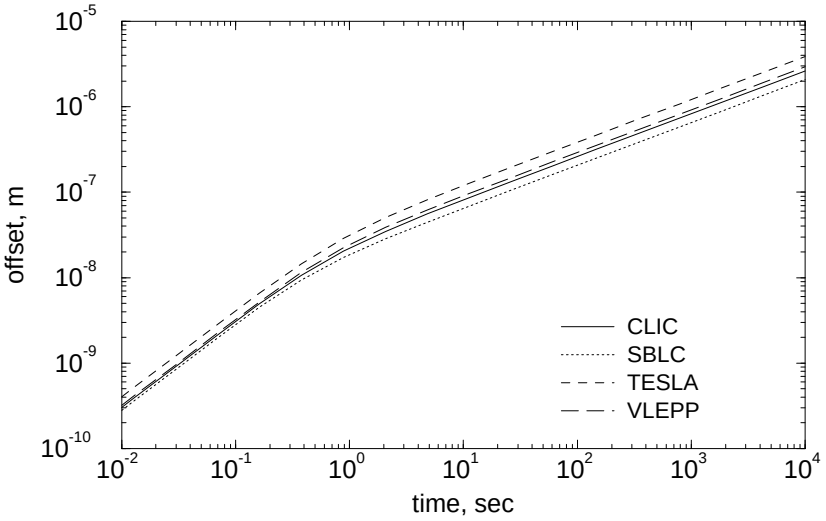

Figure 11: Expected relative vertical offset of the beams at the IP versus time for the FFS of different linear colliders.

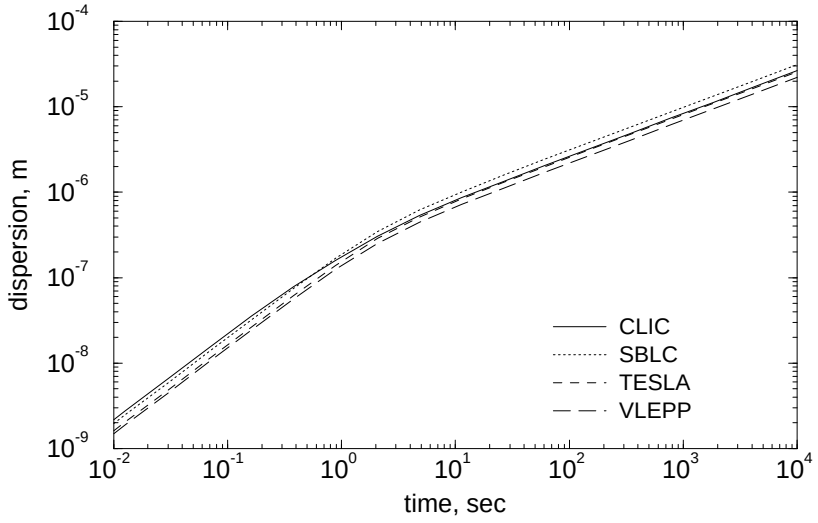

Figure 12: Expected vertical dispersion at the IP versus time for the FFS of different linear colliders.

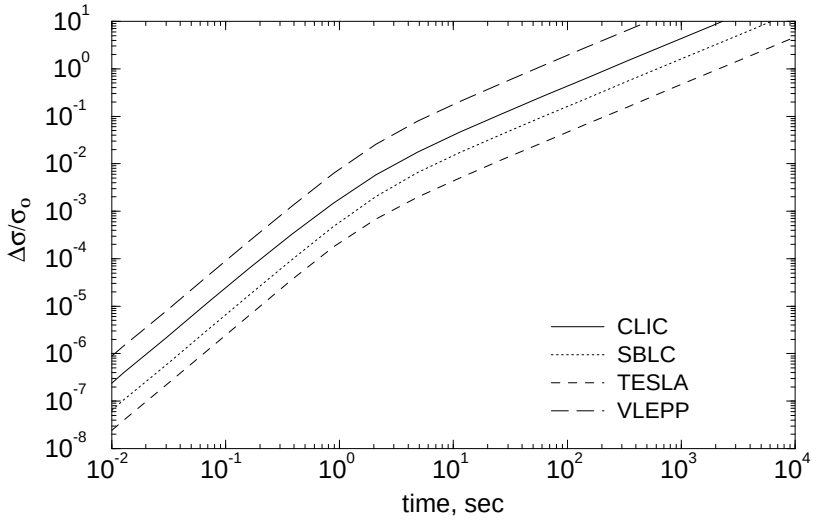

Figure 13: Spot size growth at the IP versus time for the FFS of different linear colliders.

ten times smaller than for the two preceding spectra. It is then interesting to resume the analysis of the sensitivity of final focus systems for these spectra and to compare it with the previous results. This is done in Fig.14 and Fig.15 for the vertical offset and vertical dispersion at the IP of the TESLA FFS.

In these plots, curve (1) corresponds to the quiet spectrum given by Eq.(28), curve (2) to the spectrum given by Eq.(34) with the 4 additional waves (one from the ocean and three local ones) and $A = 10^{-4}$ μm^2/sec/m, while curve (3) should describe more accurately the conditions prevailing at DESY with the same waves and $A = 10^{-5}$ μm^2/sec/m. The approximation with only the additional contribution of waves from the ocean gives the same results as curves (1) within 2%. This can be explained by the fact that these waves are very well correlated.

These comparisons show that the impact of the cultural noise is very important for the short time correction of the offset jitter, and is negligible for the long time correction of the dispersion. For TESLA the tolerance on the vertical dispersion from 2% luminosity loss is around 4 μm: it is therefore set by the ATL part of the spectrum. On the contrary, the tolerance on the offset is around 5 nm and corresponds to the offset predicted after only 1 msec, that is roughly the length of one bunch train. This means that a continuous offset correction inside of the bunch train would just start to be required for a higher level of local noise.

The effect of the local cultural waves appears also clearly in the integral of the spectral function $G(k)$ for the relative offset

$$\int_0^k \frac{dk'}{2\pi} \int_0^\infty P(\omega, k')\, G(k')\, 2(1 - cos(\omega T))\, \frac{d\omega}{2\pi} \tag{58}$$

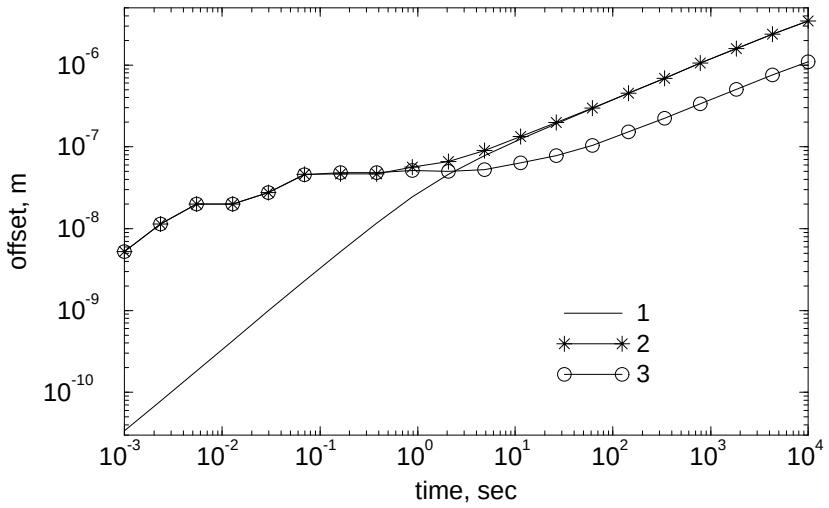

Figure 14: Expected vertical relative offset of the beams at the IP for the TESLA FFS for different models of the power spectrum $P(\omega, k)$.

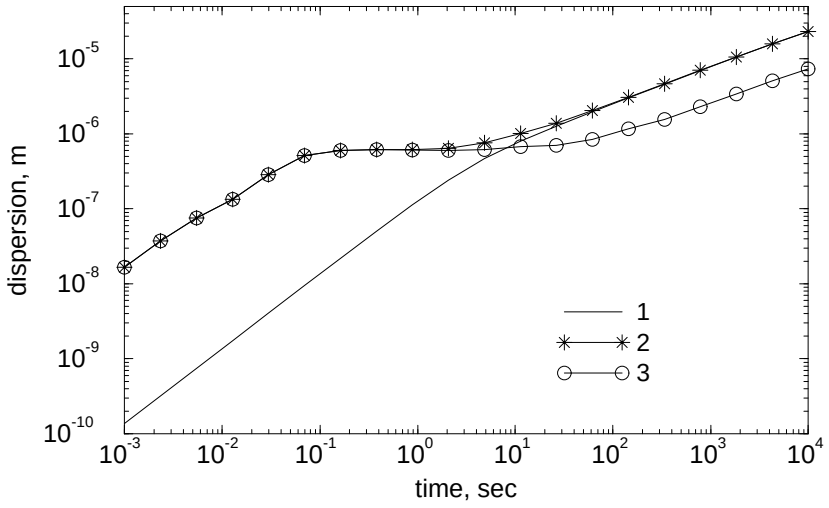

Figure 15: Expected vertical dispersion at the IP of the TESLA FFS for different models of the power spectrum $P(\omega, k)$.

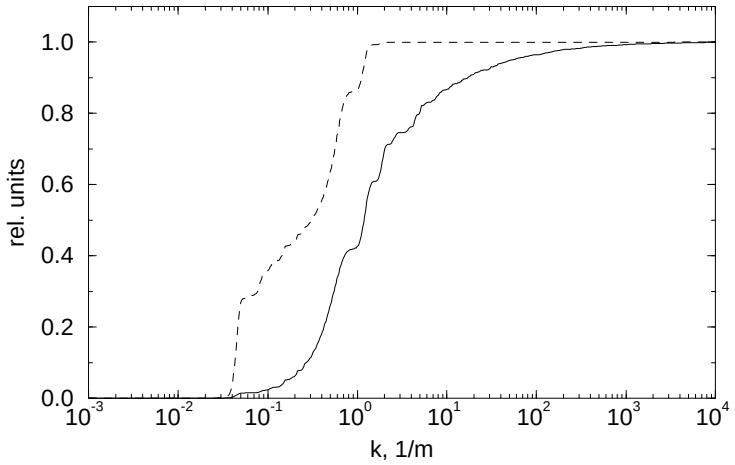

Figure 16: Normalized integrated contribution of spatial harmonics up to the wake number k to the offset of the beams at IP of the TESLA FFS for $T = 0.03$ s. Solid line: quiet spectrum, dashed line: HERA spectrum.

up to a given wave number k and normalized by its total integral i.e. by the rms offset according to Eq.(46). This integral is plotted in Fig.(16) for the quiet and HERA seismic conditions for TESLA after a time $T = 0.03$ s. The regions of wave numbers where it increases rapidly are therefore the most harmful ones. It is clear that the local waves of the HERA spectrum contribute mostly in the region of wavelengths around 10 meter comparable to the lattice periods and beta-functions. This is of course the most dangerous region.

5 Conclusion

The influence of ground motion is expected to be very important for the future TeV linear colliders. It will require precise alignment techniques probably combined with damping of the magnet vibrations. To describe this influence quantitatively in terms of beam properties and luminosity at the IP, we propose to use the power spectrum $P(\omega, k)$, previously introduced by one of the author. This two dimensional power spectrum describes both the time and spatial properties of ground motion. It also encompasses the power spectra associated to the absolute and to the relative displacements such as the ATL law describing slow diffusive motion. Various expressions of this spectrum can be built to modelize the information about absolute and relative measurements of ground motion. We have derived two such models to account for typical low or high cultural noise conditions.

We then described the formalism which allows to express the time evolution of

typical beam properties, such as beam offset, dispersion or spot size, for a beam line submitted to transverse vibrations corresponding to a given power spectrum $P(\omega, k)$ of ground motion. Finally we applied this formalism to analyze the sensitivity of various final focus systems for linear collider designs to ground vibrations over short and long time ranges, using and comparing the power spectra for quiet and noisy conditions.

Acknowledgement

The authors would like to thank Stéphane Fartoukh for help in the calculations, John Irwin and Vladimir Shiltsev for useful discussions and Vladimir Balakin for interest in the work.

References

[1] Proceedings of the International Workshops on Linear Colliders LC89-95.

[2] *Linear Collider Technical Review*, To be published.

[3] L. Hendrickson et al *Tutorial on Beam-Based Feedback Systems for Linacs*, SLAC-PUB-6621, August 1994

[4] Fischer G.E. *Ground Motion and its Effects in Accelerator Design*, Standford, 1985; SLAC-PUB-3392 Rev., July 1985.

[5] Baklakov B.A., Lebedev P.K., Parkhomchuk V.V., Sery A.A., Sleptsov A.I., Shiltsev V.D. *Investigation of Correlation and Power Characteristics of Earth Surface Motion in the UNK Complex Region*, INP Preprint 91-15, Novosibirsk 1991 (in Russian).

[6] Lebedev V.A., Lebedev P.K., Parkhomchuk V.V., Shiltsev V.D. *Transverse Vibrations of Electron Beam and Ground Motion Measurements at VEPP-3 Storage Ring*, INP Preprint 92-39, Novosibirsk, 1992.

[7] Juravlev V.M., Sery A.A., Sleptsov A.I., Coosemans W., Ramseier G., Wilson I. *Investigation of Power and Spatial Characteristics of Seismic Vibrations in the CERN LEP Tunnel for Linear Collider Studies*, CERN SL/93-53, CLIC-Note 217.

[8] Takeda S., Akiyama A., Kudo K., Nakanishi H., Yamamoto N. *Slow Drift and Frequency Spectra on Ground Motion*, KEK Preprint 93-61, July 1993.

[9] Shiltsev V. *Seismic Measurements at DESY*, report on LC95 Workshop, Tsukuba, 1995, unpublished.

[10] Juravlev V.M., Lunev P.A., Sery A.A., Sleptsov A.I., Honkavaara K., Orava R., Pietarinen E. *Seismic Conditions in Finland and Stability Requirements for the Future Linear Collider*, HU-SEFT R 1995-01, Helsinki 1995.

[11] Adolphsen C., Ross M. *SLC Linac Vibration Study*, report on LC95 Workshop, Tsukuba, 1995, unpublished.

[12] Rossbach J. *Fast Ground Motion at HERA*, DESY 89-023, February 1989.

[13] Parkhomchuk V., Shiltsev V., Weaver H.J. *Measurements of Ground Motion Vibrations at the SSC*, SSCL Preprint 323, May 1993.

[14] Baklakov B.A., Lebedev P.K., Parkhomchuk V.V., Sery A.A., Sleptsov A.I., Shiltsev V.D. *Investigation of Seismic Vibrations for the Linear Collider VLEPP*, Journal of Technical Physics, Vol.63, N 10, p.122-131, 1993 (in Russian).

[15] Parkhomchuk V., Shiltsev V., Stupakov G. *Slow Ground Motion and Operation of Large Colliders*, Particle Accelerators Vol. 46, No. 4, p.241 (1994).

[16] Parkhomchuk V., Shiltsev V. *Fractal Model of the Ground Motion*, Preprint INP 92-31, Novosibirsk, 1992 (in Russian).

[17] Brinkmann R., Rossbach J. *Observation of Closed Orbit Drift at HERA Covering 8 Decades of Frequency*, Nuclear Instruments and Methods in Physics Research, A 350, p.8-12, (1994).

[18] Napoly O., Klein E., Rifflet J. *TESLA Final Focus System with Superconducting Magnets in the Interaction Region: Optics, Tolerances and Magnet Design*, DAPNIA/94-10, CE Saclay, 1994.

[19] Fischer G.E., Morton P. *Ground Motion Tolerances for the SSC*, SSC-55, 1986.

[20] Brown K.L., Murray J.J., Fieguth T. *The Completed Design of the SLC Final Focus System*, SLAC-PUB-4219, 1986.

[21] Napoly O., Taylor T., Zotter B. *A Final Focus Design for the CERN Linear Collider CLIC*, CERN, CH-1211, 1989.

[22] Sery A., Napoly O. *Calculations of influence of the ground motions on the TESLA with new set of parameters*, TESLA workshop at Gran-Sasso, Italy, May 1995, unpublished.

[23] Shiltsev V., Baklakov B., Lebedev P., Rossbach J., Montag C. *Measurements of Ground Vibrations and Orbit Motion at HERA*, DESY HERA 95-06, June 1995.